IEEE Open Access Journal of
Power and Energy

Received 14 September 2023; revised 13 December 2023; accepted 7 January 2024.
Date of publication 16 January 2024; date of current version 23 February 2024.

Digital Object Identifier 10.1109/OAJPE.2024.3354079

Adaptive Voltage Reference Based Controls of Converter Power Sharing and Pilot Voltage in HVDC System for Large-Scale Offshore Wind Integration

YUANSHI ZHANG[1,2] (Member, IEEE), WENYAN QIAN[1,2], JUN SHAO[3], FEI ZHANG[1,2] (Member, IEEE), LIWEI WANG[4] (Senior Member, IEEE), QINRAN HU[1,2] (Senior Member, IEEE), AND WEI LI[5] (Member, IEEE)

[1]School of Electrical Engineering, Southeast University, Nanjing 210096, China
[2]Jiangsu Provincial Key Laboratory of Smart Grid Technology and Equipment, Southeast University, Nanjing 210096, China
[3]School of NARI Electric and Automation, Nanjing Normal University, Nanjing 210023, China
[4]School of Engineering, The University of British Columbia Okanagan, Kelowna, BC V1V 1V7, Canada
[5]OPAL-RT Technologies, Montreal, QC H3K 1G6, Canada

CORRESPONDING AUTHOR: Q. HU (qhu@seu.edu.cn)

This work was supported in part by the National Natural Science Foundation of China under Grant 52207083 and in part by the Jiangsu Provincial Key Laboratory Project of Smart Grid Technology and Equipment (Southeast University).

ABSTRACT Active power sharing and voltage regulation are two of the major control challenges in the operation of the voltage source converter based multi-terminal high-voltage DC (VSC-MTDC) system when integrating large-scale offshore wind farms (OWFs). This paper proposes two novel adaptive voltage reference based droop control methods to regulate pilot DC voltage and share the power burden autonomously. The proposed Method I utilizes DC grid lossy model with the local voltage droop control strategy, while the proposed Method II adopts a modified pilot voltage droop control (MPVDC) to avoid the large errors caused by the DC grid lossless model. Dynamic simulations of a five-terminal MTDC grid are carried out using MATLAB/Simulink SimPowerSystems /Specialized Technology to verify the proposed autonomous control methods under various types of disturbance and contingency. In addition, comparative study is implemented to demonstrate the advantages of the proposed methods.

INDEX TERMS Adaptive voltage reference based droop, autonomous control, offshore wind farms (OWFs), power sharing, power-voltage droop control, voltage regulation, voltage source converter based multi-terminal high-voltage DC (VSC-MTDC).

I. INTRODUCTION

FACING finite fossil fuels and worldwide appeal for cutting down greenhouse gas emission, the past twenty years witness a continuous growing share of the sustainable energies in the power generation mix [1], [2], [3]. As one of the mainstream renewable energy technologies, offshore wind generation is growing rapidly in many countries in Europe, North America, and Asia [4], [5]. There are two feasible technologies to integrate the offshore wind farms into an existing AC system, i.e. high voltage ac grid and voltage source converter based high-voltage DC (VSC-HVDC) grid. However, the advantages of independent control of the active and reactive powers, undersea connection, as well as power flow redirection capability make HVDC grid, i.e. multi-terminal HVDC (MTDC) system, a preferable solution to integrate offshore wind farms [1], [6], [7], [8], [9].

The classical VSC control schemes for MTDC system can be categorized into three types: V-P control [10], voltage margin control [11], [12] and DC voltage droop control [13], [14], [15], [16], [17]. The V-P control strategy assigns a primary VSC to regulate the DC voltage while the other VSCs control real power. However, the MTDC system will be out of service when the DC voltage controlled VSC is tripped [18]. Voltage margin control is considered as an improved voltage-power control with alternative slack buses [19] although oscillation in the DC voltage profile may occur when shifting the VSC under constant voltage control [18]. The reliability and stability of the MTDC can be reinforced by distributed

droop control as multiple VSCs contribute to voltage regulation and power sharing [15], [16], [19]. There are two kinds of DC voltage droop control, namely, local voltage droop control [13], [14], [15] and pilot voltage droop control (PVDC) [20], [21], [22]. The power sharing of PVDC does not rely on local voltage following a disturbance. It is noted that the pilot voltage is selected to be the average voltage in this work. However, the drawback of PVDC, compared to the local DC voltage droop control, is its requirement on communication of pilot voltage feedback signal among the VSC stations [23].

It is critical that power burden is shared appropriately among the VSC stations after system disturbances to avoid converter overload [21] and to minimize the impact on the neighbouring AC systems. In [24] and [25], hierarchical control structures were proposed for power sharing control of MTDC system which requires communication among the VSC stations to solve global power flows of AC and MTDC system. The adaptive droop control based power sharing methods were proposed in [21], [26], and [27] while the droop control design methods for optimal power sharing were proposed in [28], [29], and [30]. However, the voltage profile of MTDC system is not regulated in these works.

Besides the power sharing control, system operators may find it important to regulate the voltages of the DC nodes, particularly for a DC system with long transmission distance and large power flow [31], [32]. DC voltage regulation is fundamental for the MTDC system operator to ensure stability, protect connected devices, control power flow, minimize losses, integrate with larger grids, manage contingencies, and enhance overall system resilience. Therefore, it is desirable to consider DC voltage control and converter power sharing simultaneously [31], [32], [33], [34], [35], [36], [37], [38], [39]. In [23], an analytical appliance to analyze the impact of the droop constants and line resistance on the post-contingency DC voltage variation and power sharing following a VSC outage was proposed. However, the method to realize the accurate power sharing was not introduced in [23]. Considering both the power sharing and the voltage deviation indexes, an adaptive droop control strategy was proposed in [33], [34], [35], and [36] to ensure that the DC-side power and voltage are within their limits. However, the DC voltages of the power controlled VSCs are not controlled and may exceed their limits. In [31], a distributed control framework was proposed to mitigate the voltage variation generated by the primary droop control and to share power equally between the VSCs. However, proportional power sharing according to the headroom was not considered in [31]. A distributed voltage control strategy was presented in [37], which can realize DC voltage control and converter power sharing with tradeoff of two conflicting control objectives [23], [37]. To be specific, if the voltages at all DC nodes are precisely regulated, it is impossible to realize accurate power sharing control [23], [37]. In comparison with frequency in the AC grid, the average voltage can manifest the overall voltage profile of the MTDC grid [20], [31]. Regulation of the pilot DC voltage to the nominal value is an effective way to refrain the DC voltages from violating the operational limit, and maintain healthy DC voltage profile especially following contingencies.

The communication required by the proposed methods is different from the global DC power flow based traditional hierarchical control [24], [26], [33], [40]. The two proposed methods do not require the communication between the secondary and primary layers since the proposed control methods do not need a centralized controller (computing center) to calculate the global DC grid power flow. Moreover, the communication needed for the two proposed control methods is much quicker and more reliable compared with that of the traditional hierarchical control in [1], [24], [25], [41], and [44]. Lastly, for the proposed Method I, only communication among the VSCs before the contingency (in order to obtain the DC nodal power and voltage) and the contingency information are needed. By contrast, communication among the VSCs in the primary layer is needed before and after the contingency for the proposed Method II because it uses the pilot (average) voltage feedback signal V_p. Since the proposed Method II removes the local voltage dependence of the power sharing following a disturbance, it is more straightforward to realize power sharing using the Method II. In addition, as the average voltage is used as the feedback signal in Method II, it is also easier to realize average voltage regulation. Consequently, the power sharing and average voltage regulation accuracy can be improved and the calculated burden can be reduced. Nevertheless, the two proposed control methods are still autonomous because the control variables (the adaptive voltage reference V_i^*) are locally/ autonomously calculated in each VSC station ([21], [22], [36], [43]).

In this paper, instead of regulating DC voltages of all the buses, desirable converter power sharing and pilot (average) voltage control are achieved simultaneously without any tradeoff, using the proposed adaptive voltage reference based droop control methods. Two novel autonomous control methods are proposed for proportional power sharing and pilot voltage regulation of an MTDC system under different types of disturbances. The key features of the presented control methods and main contributions of this work are given below:

1) Two autonomous control methods are proposed, i.e. the proposed Methods I and II. Both of the proposed methods can allocate the power burden proportionally to the converter available headroom and regulate DC grid pilot voltage simultaneously without any tradeoff. It is noted that the pilot voltage is chosen to be the average DC voltage in this work. None of the existing autonomous control methods (without a global control center to solve the optimal DC power flow) can realize power sharing and DC grid average voltage regulation simultaneously without any tradeoff. The proposed methods are viable for various types of contingencies, e.g. real power variation, converter outage, and line disconnection.

2) The proposed Method I utilizes the DC grid lossy model with the local voltage droop control strategy. In the proposed Method I, the accuracy of the steady-state analytical model of the MTDC system is improved by taking both the converter loss and grid loss variations into consideration. Thus, the accuracy of Method I is still acceptable when the DC line length changes.
3) The modified pilot voltage droop strategy (MPVDC) is introduced in the proposed Method II to compensate the big error caused by the DC grid lossless model. The MPVDC scheme can greatly reduce regulation error compared to the method using DC grid lossless model with local voltage droop control strategy and at the same time provide as much degree of freedom as the local voltage droop control for the adaptive voltage reference based droop control to realize desirable power sharing and average DC voltage control simultaneously.
4) The proposed Method II requires less computational burden than the proposed Method I as it does not need to calculate the Jacobian matrix of the DC power flow and the loss variation of the MTDC system. But, the proposed Method II needs the post-contingency communication among the VSC stations for the pilot voltage feedback signal. Moreover, the proposed control methods are much quicker and more reliable than the hierarchical control strategy in terms of communication. The calculated burden of the proposed methods is much smaller than that of the DC power flow based methods as only linear calculation is required.

II. STEADY-STATE OPERATION OF MTDC SYSTEM

In the following, the steady-state model of the VSC-MTDC system under the local voltage droop control method is introduced. The generalized DC voltage droop control equation is represented as:

$$P_i - P_i^* + R_i\left(V_i - V_i^*\right) = 0 \tag{1}$$

where P_i and P_i^* are the actual value and setpoint of injected active power for i^{th} VSC ($i\epsilon\{1,\ldots,n\}$ and n denotes the number of DC nodes), respectively; V_i and V_i^* are the actual voltage and voltage setpoint, respectively; R_i is the droop constant of the i^{th} VSC in actual value by the unit of MW/ kV, which can be calculated by

$$R_i = P_i^r k_i / V^r \tag{2}$$

where k_i is the per-unit droop constant; V^r and P_i^r are the nominal voltage and power rating. R_i is nonzero for droop controlled VSC and R_i is set to zero for a active power controlled VSC. Additionally, if a DC node is not connected to a VSC, R_i and P_i^* are both set to zero.

The DC power equation is given by

$$P_{dc,i} = V_i(\sum\nolimits_{j=1}^{n} G_{ij}V_j) \tag{3}$$

where G_{ij} is self- or mutual-conductance. Matrix format of (3) is written by

$$\mathbf{P} = \mathbf{V} \otimes (\mathbf{GV}) \tag{4}$$

where $\mathbf{P} = [P_i]_{n\times 1}$, $\mathbf{V} = [V_i]_{n\times 1}$ and $\mathbf{G} = [G_{ij}]_{n\times n}$. The symbol $\otimes$ is a Hadamard multiplication operator.

The relation between P_i and $P_{dc,i}$ is given by

$$P_i = P_{\mathrm{dc},i} + P_{C,Loss,i} \tag{5}$$

where $P_{C,Loss,i}$ is the VSC loss, which can be calculated from DC current $I_{dc,i}$ as [44]

$$P_{C,Loss,i} = a_i + b_i * I_{dc,i} + c_i * I_{dc,i}^2 \tag{6}$$

where a_i, b_i and c_i are invariable, linear and quadratic factors of $I_{dc,i}$. $I_{dc,i}$ is given by

$$I_{dc,i} = \sum\nolimits_{k=1}^{n} G_{ik}V_k \tag{7}$$

If x routes and n nodes exist in the MTDC system, $x \times n$ matrix $\mathbf{T}$ is called the incidence matrix [45]. An element of $\mathbf{T}$, i.e. T_{pq}, equals to negative one, zero or one: negative one and one denote that p^{th} line current comes in or out node q; zero indicates that the p^{th} line is not related to node q. Therefore, line voltage vector $\mathbf{U}_L$ can be expressed by

$$\mathbf{U}_L = \mathbf{TV} \tag{8}$$

The DC grid transmission loss is given by

$$P_{G,Loss} = \mathbf{U}_L^T \otimes (diag\,(\mathbf{Y}_L)\,\mathbf{U}_L) \tag{9}$$

where $\mathbf{Y}_L$ is line admittance vector [45]. The average voltage of DC grid, defined as V_{avg}, is given by

$$V_{avg} = \frac{\sum_{i=1}^{n} V_i}{n} \tag{10}$$

It is noted that the DC grid losses include two parts, i.e., the VSC loss calculated from (6) and the DC grid transmission loss calculated from (9).

III. AUTONOMOUS CONTROLS OF PILOT (AVERAGE) VOLTAGE REGULATION AND CONVERTER POWER SHARING

In order to regulate pilot (average) DC voltage and realize desirable power sharing, V_i^* in equation (1) is variable to provide extra degree of freedom, while droop constant and active power reference setpoint P_i^* are both unchanged. In this section, two novel algorithms are proposed to obtain the adaptive voltage reference autonomously. The proposed Method I is based on DC grid lossy model with local voltage droop control strategy, while a modified pilot voltage droop control strategy is proposed as an alternative method to reduce the errors caused by the DC grid lossless model.

The DC grid lossy model takes the VSC loss and DC grid transmission loss into account while the DC grid lossless model neglects these losses. Therefore, the DC grid voltages of different nodes are assumed to be identical in DC grid lossless model, while in DC grid lossy model the nodal voltages are different.

A. PROPOSED METHOD I

The proposed Method I adopts the DC grid lossy model with the local droop control strategy. The pre-contingency operating condition of the i^{th} VSC is given by (1). Following unscheduled system faults, AC power and DC voltage deviations of the i^{th} VSC are set to be ΔP_i and ΔV_i, respectively. ΔV_i^* and ΔP_i^* are the voltage and power reference variations respectively. The steady-state operating point is derived from (1) by

$$P_i + \Delta P_i - P_i^* - \Delta P_i^* + R_i\left(V_i + \Delta V_i - V_i^* - \Delta V_i^*\right) = 0 \tag{11}$$

Subtracting (11) from (1) yields

$$\Delta P_i = \Delta P_i^* + (\Delta V_i^* - \Delta V_i)R_i \tag{12}$$

It is noted that for the droop controlled VSCs, $\Delta P_i^* = 0$, while R_i and ΔV_i^* are both zero for the real power controlled VSCs.

The vector form of (12) is expressed as

$$\mathbf{\Delta P} = \mathbf{\Delta P^*} + \text{diag}(\mathbf{R})(\mathbf{\Delta V^*} - \mathbf{\Delta V}) \tag{13}$$

From (5), the deviation of active power injection from the VSC is given by

$$\Delta \mathbf{P} = \mathbf{\Delta P_{dc}} + \Delta \mathbf{P}_{C,Loss} \tag{14}$$

where $\mathbf{\Delta P_{dc}}$ and $\Delta \mathbf{P}_{C,Loss}$ are the variations of converter power injection to DC grid and converter loss, respectively.

The post-contingency operating condition of VSC loss formula (6) is given by

$$\begin{aligned} &P_{\text{C,Loss},i} + \Delta P_{C,\text{Loss},i} \\ &\quad = a_i + b_i(I_{dc,i} + \Delta I_{dc,i}) + c_i(I_{dc,i} + \Delta I_{dc,i})^2 \end{aligned} \tag{15}$$

Subtracting (15) from (6) and neglecting the quadratic variation term $c_i \Delta I_{dc,i}^2$ yield

$$\Delta P_{C,\text{Loss},i} = (b_i + 2c_i)\Delta I_{dc,i} \tag{16}$$

The variation of DC current vector $\Delta I_{dc,i}$ can be obtained from (7) by

$$\Delta I_{dc,i} = \sum\nolimits_{k=1}^{n} G_{ik}\Delta V_k \tag{17}$$

Substituting (17) into (16) and rewriting into vector form, one can obtain

$$\Delta \mathbf{P}_{C,Loss} = (\mathbf{b} + 2\mathbf{c}) \otimes (\mathbf{G}\mathbf{\Delta}\text{V}) \tag{18}$$

where $\mathbf{b} = [b_i]_{n\times 1}$ and $\mathbf{c} = [c_i]_{n\times 1}$.

The relation between the active power deviation $\mathbf{\Delta P_{dc}}$ and voltage deviation $\mathbf{\Delta V}$ can be linearized by [46]

$$\mathbf{\Delta P_{dc}} = \mathbf{J}\mathbf{\Delta V} \tag{19}$$

where $\mathbf{J}$ is the Jacobian matrix of the MTDC network. It is noted that the Jacobian matrix element is either $g_{ij}V_i$ (for $i \neq j$) or $\sum_{j=1}^{N}(g_{ij}V_j) + g_{ii}V_i$ (for $i = j$). g_{ii} and g_{ij} are self- or mutual-admittance between the two nodes.

Substituting (18) and (19) into (14) yields

$$\Delta \mathbf{P} = [(\mathbf{b} + 2\mathbf{c}) \otimes \mathbf{G} + \text{J}]\mathbf{\Delta V} \tag{20}$$

By equating $\Delta \mathbf{P}$ in (13) and (20), the DC node voltage variation can be derived by

$$\mathbf{\Delta V} = [\mathbf{J} + (\mathbf{b}+2\mathbf{c}) \otimes \mathbf{G} + \text{diag}\,(\mathbf{R})]^{-1}(\mathbf{\Delta P^*} + \text{diag}(\mathbf{R})\mathbf{\Delta V^*}) \tag{21}$$

Following the active power balance principle, one can get the following equation

$$\sum\nolimits_{j=1}^{m} \Delta P_j + \Delta P_{\Sigma}^* + \sum\nolimits_{i=1}^{n} \Delta P_{C,Loss,i} + \Delta P_{G,Loss} = 0 \tag{22}$$

where m denotes the number of VSCs in droop control scheme and $j \epsilon \{1, \ldots, m\}$; $\Delta P_{G,Loss}$ is the variation of DC grid loss; ΔP_{Σ}^* is the total power burden caused by unscheduled contingencies including fluctuation of renewable power generation and converter outage. It is noted that $\Delta P_{\Sigma}^* = \sum_{i=1}^{n} \Delta P_i^*$. Thus, (22) denotes that the power burden ΔP_{Σ}^* (together with the loss variations) caused by the contingencies are shared by the VSCs in local voltage droop control strategy. Considering (16) and (17), $\sum_{i=1}^{n} \Delta P_{C,Loss,i}$ in (22) is given by

$$\sum\nolimits_{i=1}^{n} \Delta P_{C,Loss,i} = \sum\nolimits_{i=1}^{n} [(b_i + 2c_i) \sum\nolimits_{k=1}^{n} G_{ik}\Delta V_k] \tag{23}$$

The post-contingency DC grid loss is obtained from (9) by

$$\begin{aligned} &P_{G,Loss} + \Delta P_{G,Loss} \\ &\quad = (\mathbf{U}_L + \Delta \mathbf{U}_L)^T \otimes (diag\,(\mathbf{Y}_L)\,(\mathbf{U}_L + \Delta \mathbf{U}_L)) \end{aligned} \tag{24}$$

Subtracting (24) from (9) and neglecting the quadratic variation term give

$$\Delta P_{G,Loss} = 2\Delta \mathbf{U}_L{}^T \otimes (diag\,(\mathbf{Y}_L)\,\mathbf{U}_L) \tag{25}$$

From (8), $\Delta \mathbf{U}_L$ can be obtained by

$$\mathbf{\Delta U}_L = \mathbf{T}\mathbf{\Delta V} \tag{26}$$

Substituting (26) and (8) into (25) yields

$$\Delta P_{G,Loss} = 2(\mathbf{T}\mathbf{\Delta V})^T \otimes (diag\,(\mathbf{Y}_L)\,\mathbf{TV}) \tag{27}$$

It is defined that

$$\Delta P_{\Sigma}^* + \sum\nolimits_{i=1}^{n} \Delta P_{C,Loss,i} + \Delta P_{G,Loss} = P_{mis} \tag{28}$$

As can be seen from (23) and (27), $\sum_{i=1}^{n} \Delta P_{C,Loss,i}$ and $\Delta P_{G,Loss}$ are both functions of $\mathbf{\Delta V}$. Moreover, ΔP_{Σ}^* is a known value, so that P_{mis} in (28) is also a function of $\mathbf{\Delta V}$.

The available headroom [21] of j^{th} VSC in droop control mode converter is expressed by

$$H_j = \begin{cases} P_j^r - P_j, & P_j \geq 0 \\ -P_j^r - P_j, & P_j < 0 \end{cases} \tag{29}$$

where H_j is the available headroom and P_j^r is the rated power of the converter station. Note that when real power is transmitted from DC grid to AC grid, P_j is positive.

If the power mismatch P_{mis} is shared according to available headroom H_j among the VSCs in local voltage droop control, the relation between ΔP_j and P_{mis} is obtained by

$$\Delta P_j = -P_{mis}H_j/(\sum_{j=1}^{m} H_j) \tag{30}$$

For the j^{th} droop-controlled converter in local voltage droop control ($j\epsilon\{1,\ldots,m\}$), (12) can be rewritten as

$$\Delta P_j = (\Delta V_j^* - \Delta V_j)R_j \tag{31}$$

Equating ΔP_j in (30) and (31) yields the relation between ΔV_j and ΔV_j^* as

$$\Delta V_j = \frac{P_{mis}H_j}{R_j\sum_{j=1}^{m} H_j} + \Delta V_j^* \tag{32}$$

It is noted that if all the 1^{th} to $m-1^{\text{th}}$ VSCs satisfy the power sharing constraint (30), the power mismatch ΔP_m of the m^{th} VSC in local voltage droop control is automatically shared according to its headroom. Therefore, only $m-1$ number of equality constraints are needed for the power sharing control. If all the voltage references ΔV_j^* are set to be adaptive, one remaining degree can regulate average DC voltage. The following expression of post-contingency DC average voltage regulation is written as

$$\Delta V_{avg} = \frac{\sum_{i=1}^{n}\Delta V_i}{n} = V_{avg,sch} - V_{avg,pre} \tag{33}$$

where ΔV_{avg} is the average voltage variation; $V_{avg,sch}$ and $V_{avg,pre}$ are the scheduled and initial average DC voltages.

Considering (32) and (33), the equation set to realize power sharing control and average voltage regulation is given by

$$\begin{bmatrix} \Delta V_1 \\ \vdots \\ \Delta V_{m-1} \\ \frac{\sum_{i=1}^{n}\Delta V_i}{n} \end{bmatrix} = \begin{bmatrix} \frac{P_{mis}H_1}{R_1\sum_{j=1}^{m}H_j} + \Delta V_1^* \\ \vdots \\ \frac{P_{mis}H_{m-1}}{R_{m-1}\sum_{j=1}^{m}H_j} + \Delta V_{m-1}^* \\ V_{avg,sch} - V_{avg,pre} \end{bmatrix} \tag{34}$$

Finally, the DC voltage reference variation vector $\mathbf{\Delta V^*}$ can be calculated by combining (21) and (34).

B. PROPOSED METHOD II

In the ideal DC grid lossless model [33], [46], the DC voltages are assumed to be identical. Thus, (31) can be rewritten as

$$\Delta P_j = (\Delta V_j^* - \Delta V)R_j \tag{35}$$

where ΔV is the identical voltage variation.

This DC lossless model for the MTDC grid in local voltage droop control strategy is a useful tool to estimate the power distribution of the MTDC system following a disturbance. However, it may involve large errors in post-contingency DC power and voltage estimation as the DC voltage in (25) is assumed to be identical [33], [46]. In [33] and [46], the authors point out that the ideal lossless model results in large errors when calculating the changes in DC voltages and powers. In addition, the errors are affected by the values of droop coefficients, line resistances, and types of the contingency.

The PVDC is expressed as

$$P_j - P_j^* + R_j\left(V_p - V_p^*\right) = 0 \tag{36}$$

where V_p is the pilot voltage feedback signal while V_p^* is its reference value [20], [21], [22]. It is noted that the pilot voltage V_p can be selected as the voltage of a certain pilot DC bus or a combination of several DC buses. In the presented work, V_p can be assumed to be DC grid average voltage to facilitate the average voltage regulation.

Using the PVDC can avoid the large errors involved in the local voltage droop control strategy with the DC grid lossless model, because active power sharing of a pilot voltage feedback signal does not rely on the local voltage following a contingency [23]. The relationship between power variation ΔP_j and pilot voltage variation ΔV_p is given by

$$\Delta P_j = (\Delta V_p^* - \Delta V_p)R_j \tag{37}$$

Comparing (35) and (37), setting V_j^* of all the droop- controlled converters to be adaptive in (35) can provide m degree of freedom, while setting V_p^* to be adaptive in (37) can only provide one degree of freedom. Thus, the disadvantage of the PVDC is that it lacks degree of freedom for the adaptive droop control.

In this work, a modified pilot voltage droop control (MPVDC) is proposed, which is given by

$$P_j - P_j^* + R_j\left(V_p - V_j^*\right) = 0 \tag{38}$$

The relationship between power variation ΔP_j and pilot voltage variation ΔV_p in the MPVDC is given by

$$\Delta P_j = (\Delta V_j^* - \Delta V_p)R_j \tag{39}$$

As the control target of the proposed control method is the voltage reference regulation, degree of freedom is computed according to the number of the voltage reference in the MTDC system. The PVDC method has only one degree of freedom since the pilot voltage variation ΔV_p^* in (37) is the same for all the droop controlled nodes. However, the MPVDC method possesses much more degree of freedom since the local voltage variation ΔV_j^* can be different for all the droop controlled VSCs. Therefore, comparing (39) with (35) and (37), it can be seen that the MPVDC avoids the large errors involved in the DC grid lossless model with local voltage droop control and at the same time provides as much degree of freedom as the local voltage droop control.

Following the active power balance relationship, one can obtain

$$\sum_{j=1}^{m}\Delta P_j + \Delta P_\Sigma^* = 0 \tag{40}$$

Substituting (39) into (40) gives

$$\Delta V_p = (\sum_{j=1}^{m} \Delta V_j^* R_j + \Delta P_\Sigma^*)/(\sum_{j=1}^{m} R_j) \tag{41}$$

Substituting (41) into (39) yields

$$\Delta P_j = [\Delta V_j^* - (\sum_{j=1}^{m} \Delta V_j^* R_j + \Delta P_\Sigma^*)/\sum_{j=1}^{m} R_j]R_j \tag{42}$$

Equating (30) and (42) yields the following equation system:

$$\begin{bmatrix} \Delta V_1^* \\ \Delta V_2^* \\ \vdots \\ \Delta V_m^* \end{bmatrix} = \begin{bmatrix} (\sum_{j=1}^{m} \Delta V_j^* R_j + \Delta P_\Sigma^*)/\sum_{j=1}^{m} R_j \\ (\sum_{j=1}^{m} \Delta V_j^* R_j + \Delta P_\Sigma^*)/\sum_{j=1}^{m} R_j \\ \vdots \\ (\sum_{j=1}^{m} \Delta V_j^* R_j + \Delta P_\Sigma^*)/\sum_{j=1}^{m} R_j \end{bmatrix} - \begin{bmatrix} \frac{\Delta P_\Sigma^* H_1}{R_1(\sum_{j=1}^{m} H_j)} \\ \frac{\Delta P_\Sigma^* H_2}{R_2(\sum_{j=1}^{m} H_j)} \\ \vdots \\ \frac{\Delta P_\Sigma^* H_m}{R_m(\sum_{j=1}^{m} H_j)} \end{bmatrix} \tag{43}$$

It can be seen from the right side of (43) that the same term $(\sum_{j=1}^{m} \Delta V_j^* R_j + \Delta P_\Sigma^*)/\sum_{j=1}^{m} R_j$ is included in every equation. Therefore, (43) can be simplified by subtracting j^{th} row ($j \epsilon \{1, \ldots, m-1\}$) from $j+1^{\text{th}}$ row and m^{th} row from the 1^{st} row in (11), which yields the equivalent equation set

$$\begin{bmatrix} \Delta V_1^* - \Delta V_2^* \\ \Delta V_2^* - \Delta V_3^* \\ \vdots \\ -\Delta V_1^* + \Delta V_m^* \end{bmatrix} = - \begin{bmatrix} \frac{\Delta P_\Sigma^*}{\sum_{j=1}^{m} H_j}(\frac{H_1}{R_1} - \frac{H_2}{R_2}) \\ \frac{\Delta P_\Sigma^*}{\sum_{j=1}^{m} H_j}(\frac{H_2}{R_2} - \frac{H_3}{R_3}) \\ \vdots \\ \frac{\Delta P_\Sigma^*}{\sum_{j=1}^{m} H_j}(\frac{H_m}{R_m} - \frac{H_1}{R_1}) \end{bmatrix} \tag{44}$$

Extracting the coefficient matrix of (44) yields

$$\begin{bmatrix} 1 & -1 & 0 & \cdots & 0 \\ 0 & 1 & -1 & & 0 \\ & \vdots & & \ddots & \vdots \\ -1 & 0 & 0 & \cdots & 1 \end{bmatrix}_{m \times m} \tag{45}$$

As the rank of the $m \times m$ matrix (45) is $m-1$, matrix (45) is not a full rank matrix. Thus, there are non-unique solutions of (44). In other words, one degree of freedom exists in (44). Therefore, we can utilize this additional degree of freedom to regulate the DC average voltage. It is noted that the average voltage can be selected to be pilot voltage feedback signal V_p. Combining (33) and (41) gives

$$\frac{\sum_{j=1}^{m} \Delta V_j^* R_j + \Delta P_\Sigma^*}{\sum_{j=1}^{m} R_j} = V_{avg,sch} - V_{avg,pre} \tag{46}$$

Substituting (46) into (43), one can get the equation set with a unique solution as

$$\begin{bmatrix} \Delta V_1^* \\ \Delta V_2^* \\ \vdots \\ \Delta V_m^* \end{bmatrix} = \begin{bmatrix} V_{avg,sch} - V_{avg,pre} \\ V_{avg,sch} - V_{avg,pre} \\ \vdots \\ V_{avg,sch} - V_{avg,pre} \end{bmatrix} - \begin{bmatrix} \frac{\Delta P_\Sigma^* H_1}{R_1(\sum_{j=1}^{m} H_j)} \\ \frac{\Delta P_\Sigma^* H_2}{R_2(\sum_{j=1}^{m} H_j)} \\ \vdots \\ \frac{\Delta P_\Sigma^* H_m}{R_m(\sum_{j=1}^{m} H_j)} \end{bmatrix} \tag{47}$$

C. CONTROL SCHEME DIAGRAM

The control diagram of the presented autonomous converter power sharing and average DC voltage control is shown in Fig. 1. The physical layer is composed of offshore wind farms (OWFs), wind farm VSCs (WFVSCs), AC grids, grid-side VSCs (GSVSCs) and the MTDC system. The primary control layer comprises outer power control, inner current control (ICC) and the pulse width modulation (PWM). It is assumed that the WFVSCs are in real power control and AC voltage magnitude control modes for the d-axis and q-axis controls, respectively. The GSVSCs are in adaptive voltage reference based droop control and reactive power control modes for the d-axis and q-axis controls, respectively. The reference values of the d-axis and q-axis currents, i.e. i_d^* and i_q^*, are transmitted from the outer power controls to the ICCs.

It is noted that the adaptive V^* is generated from the presented autonomous control layer and is calculated using either the proposed Method I or II, as shown Fig. 1 by the switch position I or II, respectively. In the autonomous control layer, the output voltage reference variation $\Delta \mathbf{V^*}$ is smoothed by a ramp process before transmitting to the primary layer to avoid large transient.

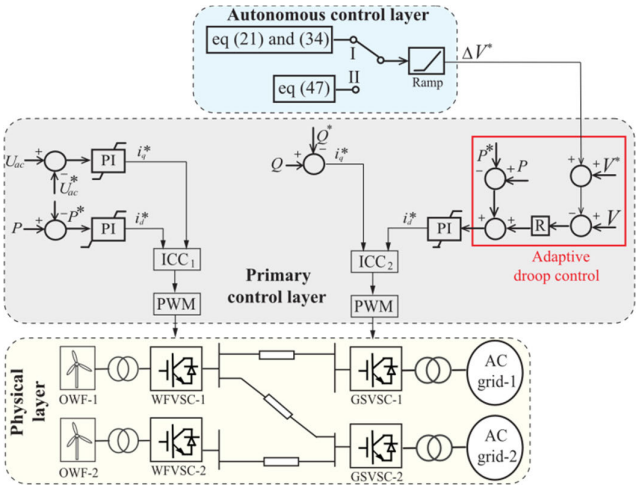

FIGURE 1. Control scheme diagram of the proposed autonomous control strategy.

D. DISCUSSION

In order to compare the power sharing accuracy of the proposed Methods I and II, the active power sharing error, i.e. P_{err}, is given as

$$P_{err} = \left\| \Delta \mathbf{P} - \left(-\frac{\mathbf{H} P_{mis}^{ref}}{\sum_{j=1}^{m} H_j}\right) \right\|_1 / P^r \tag{48}$$

where P^r is the nominal power of the GSVSCs (since all the GSVSCs in the case study have the same power rating); $\mathbf{H}$ is vector of the available headroom ($\mathrm{H} = [H_1, \cdots H_m]$). It is noted that P_{mis}^{ref} is obtained by the accurate MTDC grid power flow result following the method proposed in [44] and is used as the benchmark in this work.

The average voltage regulation error V_{err} is given by

$$V_{err} = \left| V_{avg,sch} - V_{avg,post} \right| / V^r \tag{49}$$

where $V_{avg,sch}$ and $V_{avg,post}$ are the scheduled average voltage and post-contingency average voltage, respectively.

It is noted that Method II is derived from (35). Based on the DC grid lossless, ΔV is the identical voltage variation. This will cause big errors using the traditional voltage droop control. However, under the proposed MPDC in (39), the pilot voltage feedback signal ΔV_p is identical without any assumption. Consequently, although Method II derives from the DC grid lossless model, the errors are only caused by neglecting the converter and grid loss variations in (40). The converter and grid losses are around 2% of the DC rated power and their variations are around 0.2% of the DC rated power, which is negligible. While the errors, P_{err} and V_{err}, of the proposed Method I are due to the linearization of MTDC power flow in (19). Thus, the proposed Method II is more accurate than Method I.

It is also noted that the calculated burden of the Method II is much lower than that of the proposed Method I since the proposed Method II avoids calculating the Jacobian matrix $\mathbf{J}$ and variations of DC grid and converter losses. However, the proposed Method II needs the communication among different VSC stations as the pilot voltage feedback signal V_p is used in the proposed MPVDC strategy.

Four kinds of unpredicted disturbances are considered in the presented work, i.e. real power variation caused by the OWF power generation intermittency, real-power-controlled converter outage, droop-controlled converter outage, and DC line disconnection. It is straightforward to set $\Delta \mathbf{P}^*$ in (21) and ΔP_{Σ}^* in (22) for the first two types of disturbances. For the droop-controlled converter outage, the droop constant of the tripped converter is set to be zero before the contingency to keep diag($\mathbf{R}$) in (21) unchanged before and after the contingency.

In the following, the method to set $\Delta \mathbf{P}^*$ and ΔP_{Σ}^* following DC line disconnection is discussed in detail. Assume that the line is tripped in the initial state and two dummy generators are installed at two ends of disconnected line, respectively. The real power of the dummy generators is the same as the original line power injections. Thus, the topology change caused by a line disconnection is converted to real power variations of the two DC nodes. The corresponding elements in $\Delta \mathbf{P}^*$ are the negative values of the line power injections while ΔP_{Σ}^* equals to the initial copper loss of the disconnected transmission line.

Method II is more accurate than Method I and has less calculated burden. In addition, since Method II is based on the novel MPVDC proposed in this work, it is more straightforward to derive the power sharing and voltage regulation. However, the Method II needs post-contingency communication since it is a common feedback signal based method. Therefore, if the post-contingency communication in the primary layer is lost, Method I will be selected instead of Method II.

IV. CASE STUDIES

A. SIMULATION SYSTEM CONFIGURATION

A five-terminal VSC-MTDC system with OWFs is used to verify the proposed autonomous controls of converter power sharing and DC pilot (average) voltage control, as shown in Fig. 2. The MTDC grid is implemented using MATLAB/Simulink SimPowerSystems /Specialized Technology Blockset and OPAL-RT RT-LAB libraries. Two OWFs and three AC systems are connected to the MTDC system at VSCs-3 and the other three VSCs, respectively. The WFVSCs are under real power control scheme, while the GSVSCs are under DC voltage droop control strategy. Each VSC is represented by average-value model [47], [48], [49] of modular multilevel converter (MMC).

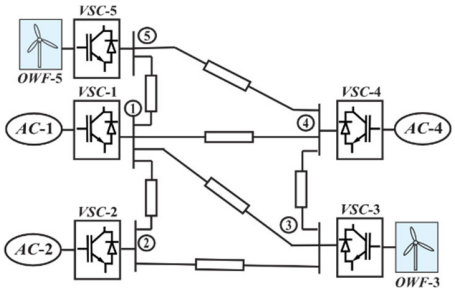

FIGURE 2. **Single line diagram of the test system.**

The DC cables are modelled using RT-LAB/ARTEMiS Blockset. The DC cable length and parameters as well as VSC station parameters are shown in Tables 1 to 3, repectively. The VSCs-1 and 2 are implemented using MMC with half-bridge submodules, while the other VSCs are implemented using MMC with full-bridge submodules. The converter loss coefficients in (6) are given in Table 4 [44]. The upper and lower DC voltage limits are 380 kV and 420 kV, respectively.

In the initial state, the WFVSC-3 changes from −750 MW to −400MW due to wind power variation.

The effectiveness of the presented autonomous control methods is verified using wind farm generation increase and decrease in Cases *A and D*, respectively. Case *B* is a comparative study, which demonstrates that the advantages of the

TABLE 1. DC cable length.

DC cable	1 to 2	1 to 3	1 to 4	1 to 5	2 to 3	3 to 4	4 to 5
Length (*km*)	160	400	250	320	320	320	500

TABLE 2. DC cable parameter.

Parameter	R(Ω/km)	L(mH/km)	C($\mu F/km$)
Value	0.0200	0.1463	0.2662

TABLE 3. VSC station parameter.

VSC No.	1	2	3	4	5
Nominal Voltage V_i^r (kV)	400	400	400	400	400
Rated Power P_i^r (MW)	500	500	800	500	900
Droop Coefficient k_i (IN P.U.)) [33]	0.1	0.0668	0	0.04	0
Power Reference P_i^* (MW)	350	500	−750	400	−500

TABLE 4. Per-unit VSC loss coefficients [44].

Submodule Type	a_{dc}	b_{dc}	c_{dc}	
Half-bridge Full-bridge	8.80	4.00 6.70	0.47 0.96	$\times 10^{-3}$

proposed Methods I and II compared with the Method III proposed in [33] under GSVSC failure. Method III [33] introduces an adaptive droop control scheme incorporating both the DC voltage deviation factor and the power sharing factor. This scheme is designed to guarantee that the DC voltage and power loading rate of only the converter under droop control remain within their specified limits. In Case *C*, performance of the presented autonomous control methods to realize average DC voltage control and proportional converter power sharing is verified under $N-2$ contingency. Case *E* compares the dynamic response of the MTDC system after a disturbance with and without automatic control

B. CASE A: POWER DECREASE OF OWF GENERATION

Case *A* shows that the presented autonomous controls are able to share power proportionally and regulate DC average voltage to the nominal value under wind power generation increase. In Case *A*, the active power of the VSC Station 5 goes up from −500 MW to −850 MW when the time is 0.5 second. The autonomous controls are enabled at t = 1s.

The DC powers, voltages and average voltage of VSCs under the proposed Methods I and II are given in Figs. 3 and 4, respectively. It can be seen from Figs. 3 and 4 that autonomous controls in Methods I and II produce similar results with small errors (shown in Table 5).

TABLE 5. Comparison of methods I and II under power variation.

Method	I	II
V_{err} (%)	0.09	0.02
P_{err} (%)	1.63	0.70

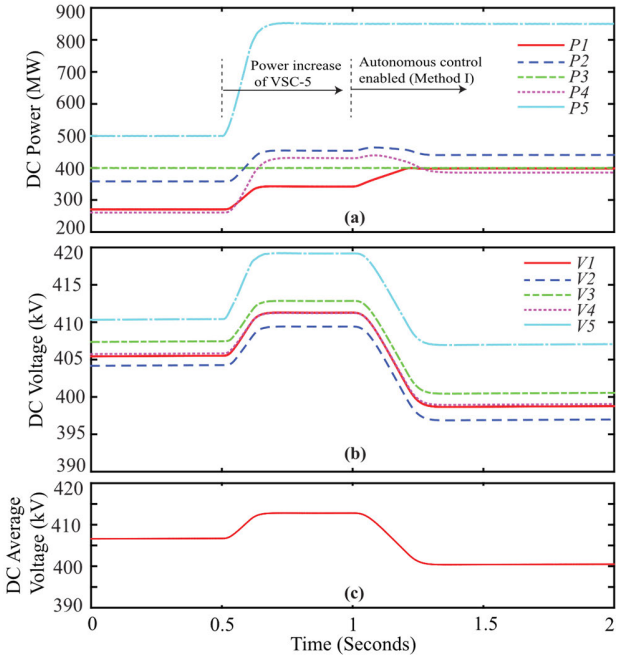

FIGURE 3. DC powers, voltages and average voltage of VSCs when VSC-5 power increases under the proposed Method I. (a) VSC active powers; (b) VSC DC-side voltages; (c) VSC average voltage.

From Figs. 3 (a) and 4 (a), one can see that when the active power of VSC-5 goes up, the distribution of active power of the VSCs-1, 2 and 4 under the traditional droop is not desirable as VSC-1 still has relatively large headroom compared with the other two droop-controlled VSCs. After the proposed autonomous controls are activated at t = 1s, the active powers of the GSVSCs are shared proportionally to their headrooms. On the other hand, it is observed from Figs. 3 (b) and 4 (b) that the DC voltage profile increases following the active power variation of the VSC-5. Especially, DC voltage of the VSC-5 is close to the upper voltage limit (420kV). As shown in Figs 3 (c) and 4 (c), the voltage profile increase is mitigated after the autonomous controls are activated to adjust the average voltage to the nominal value. It is observed from Table 5 that V_{err} and P_{err} of the proposed Method II are smaller than those of the proposed Method I, indicating the proposed Method II is more accurate than the proposed Method I. This is because the error due to neglecting the converter and grid loss variations in (40) of the proposed Method II is smaller than the linearization error of MTDC power flow in (19) of the proposed Method I.

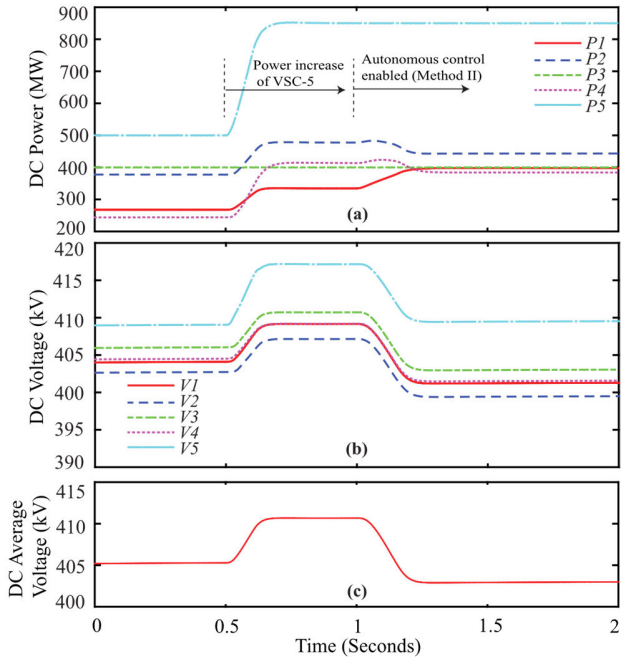

FIGURE 4. DC powers, voltages and average voltage of VSCs when VSC-5 power increases under the proposed Method II. (a) VSC active powers; (b) VSC DC-side voltages; (c) VSC average voltage.

C. CASE B: COMPARATIVE STUDY OF GSVSC OUTAGE

In this situation, the presented autonomous control strategies are contrasted with the Method III proposed in [33] when the MTDC grid encounters huge perturbation, i.e. GSVSC failure. The Method III proposed in [33] can guarantee the active power and voltage of all the droop controlled VSCs below their boundaries. However, the DC voltages of the power controlled VSCs under the Method III are not regulated and may exceed their limits.

1) THE PROPOSED METHODS I AND II

In Case B, the proposed autonomous control methods are applied to share power proportionally and regulate average DC voltage under the GSVSC outage. In this case, VSC-2 is tripped at t = 0.5s. The presented autonomous controls are enabled at t = 1s. It is seen from Table 6 that the proposed Methods I and II are able to realize the voltage control and active power sharing control with small errors. Similar to Case A, Method II is more accurate than Method I. Due to space limitation, only the DC powers, voltages, and average voltage of VSCs of the presented Method I are shown in Fig. 5.

It is shown in Fig. 5 (a) that the active power of VSC-4 is fully-loaded under the VSC-2 failure, while VSC-1 still has plenty of headroom. After the autonomous control is enabled, the active power burden caused by VSC-2 outage is proportionally distributed by VSCs-1 and 4 according to their headrooms. It is illustrated in Figs. 5 (b) and (c) that obvious voltage increase occurs in the voltage profile when

TABLE 6. Comparison of methods I and II under converter outage.

Method	I	II
V_{err} (%)	0.15	0.03
P_{err} (%)	1.97	0.73

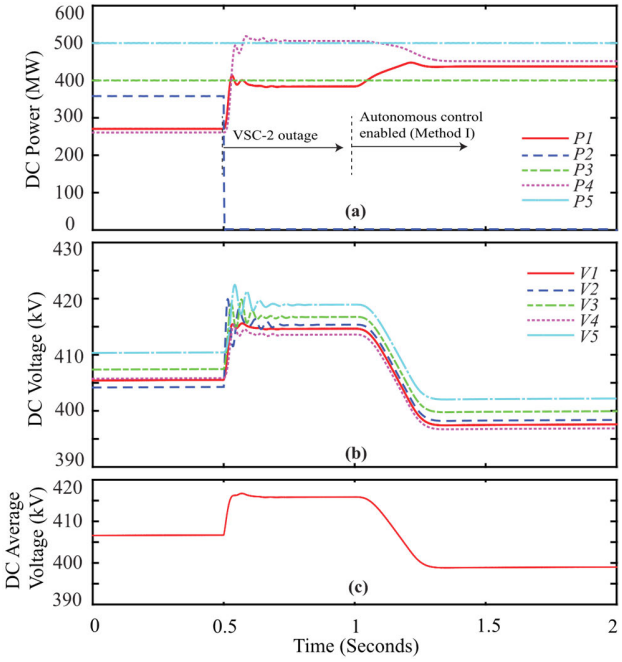

FIGURE 5. DC powers, voltages and average voltage of VSCs when VSC-2 is tripped under the proposed Method I. (a) VSC active powers; (b) VSC DC-side voltages; (c) VSC average voltage.

VSC-2 breaks down at t = 0.5s. After the presented control is enabled at t = 1s, the increase of DC voltage profile is mitigated while the average voltage is adjusted to 420 kV.

2) THE METHOD III PROPOSED IN [33]

The simulation result under the Method III proposed in [33] is shown in Fig. 6. Similarly, VSC-2 breaks down at t = 0.5s. Then autonomous control of Method III is enabled at t = 1s.

It is shown from Fig. 6 (a) that, active powers of VSCs-1 and 4 are both within the limit (500 MW) after the autonomous control (Method III) is activated. However, compared with Fig. 5 (a), the power sharing of Method I is more desirable than Method III as the DC power of VSC-4 in Fig 5 (a) has more headroom. In addition, as illustrated in Fig. 6 (b), DC voltage of the VSC-5 under constant P control is beyond the upper voltage limit (420kV). While in Fig. 5. (b), all the DC voltages are within the limit. Therefore, the proposed methods (Methods I and II) show better performance than Method III proposed in [33] as far as DC voltage control and active power sharing are concerned.

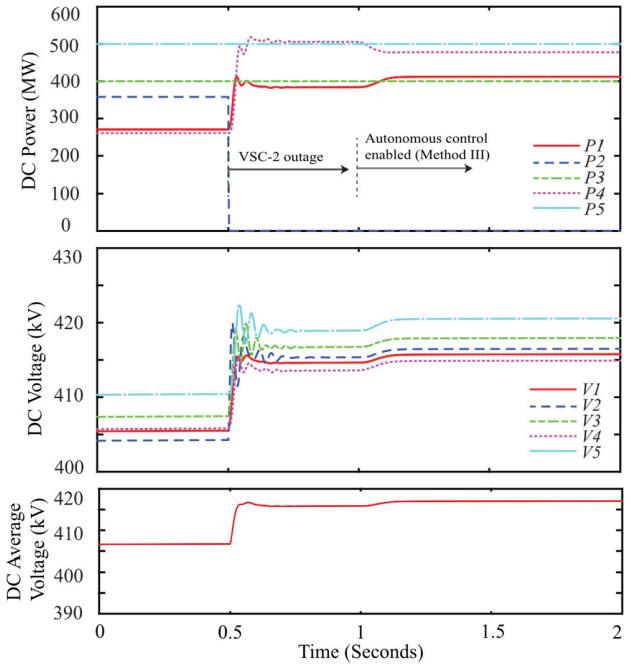

FIGURE 6. DC powers, voltages and average voltage of VSCs when VSC-2 is tripped under Method III. (a) VSC active powers; (b) VSC DC-side voltages (c) VSC average voltage.

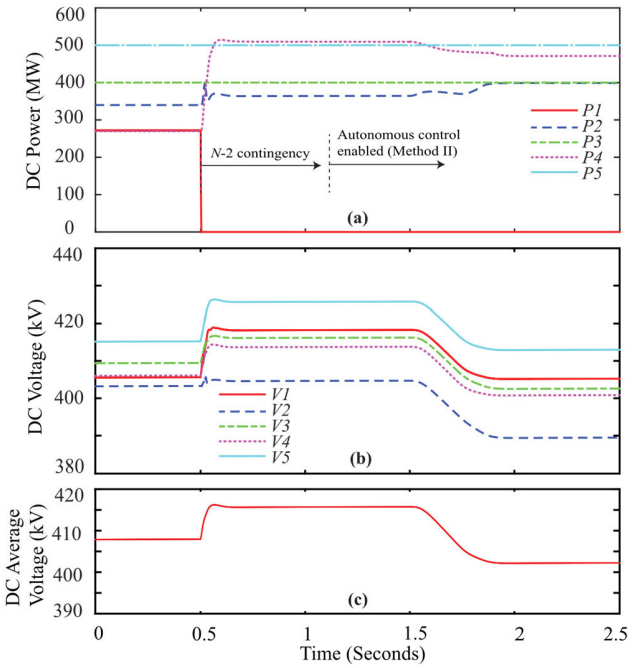

FIGURE 7. DC powers, voltages and average voltage of VSCs when VSC-1 breaks and DC line 1-2 is tripped under the proposed Method II. (a) VSC active powers; (b) VSC DC-side voltages; (c) VSC average voltage.

D. CASE C: $N-2$ CONTINGENCY

In the following, the performance of the presented autonomous control methods is validated under $N-2$ contingency. VSC-1 breaks down at t = 0.5s. Moreover, the DC line 1-2 is tripped at t = 0.5s. The presented autonomous control method is enabled at t = 1.5s. From P_{err} and V_{err} listed in Table 7, it is shown that, both of the presented methods are verified with small errors under $N-2$ disturbance. The active powers, voltages and average voltage of VSCs under the proposed Method II are shown in Fig. 7. It is illustrated from Figs. 7 (a) and (b) that, VSCs-4 is fully-loaded and VSC-5 experiences overvoltage under the fixed droop control. After the autonomous control is enabled at t = 1.5s, the DC power is shared proportionally while the average voltage is regulated close to the nominal value as shown in Fig. 7 (c). Thus, the overvoltage of the VSC stations is avoided by the proposed autonomous control methods while the active powers are shared more desirably among the VSC stations.

TABLE 7. Comparison of methods I and II under $N-2$ contingency.

Method	I	II
V_{err} (%)	0.29	0.12
P_{err} (%)	1.91	0.70

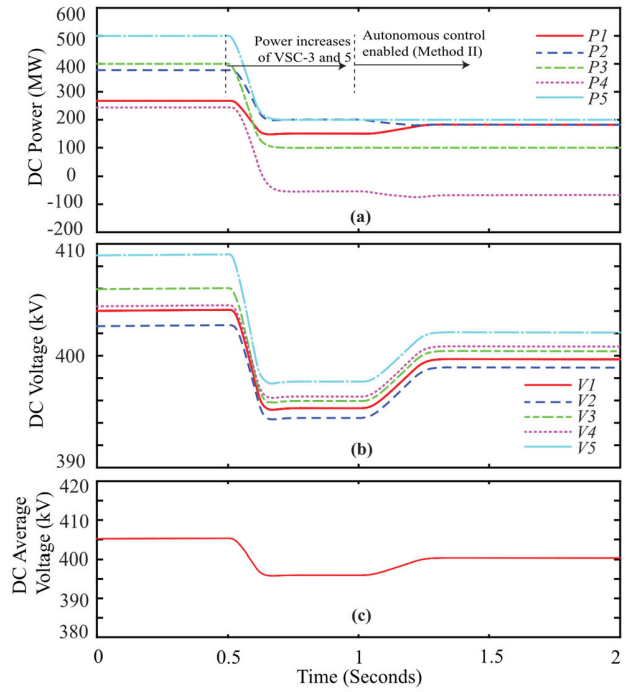

FIGURE 8. DC powers, voltages and average voltage of VSCs when VSCs-3 and 5 power decrease under the proposed Method II. (a) VSC active powers; (b) VSC DC-side voltages; (c) VSC average voltage.

E. CASE D: POWER DECREASE OF OWF GENERATION

Case D shows that the presented autonomous controls are capable of sharing power proportionally and regulating DC average voltage to the nominal value under wind power generation decrease. In Case D, the active powers of the VSC Stations 3 and 5 both decrease 300 MW when the

time is 0.5 second. The autonomous controls are enabled at t = 1s.

The DC powers, voltages and average voltage of VSCs under the proposed Methods II are given in Fig. 8. From Fig 8 (a) one can see that after the proposed autonomous controls are activated at t = 1s, the active powers of the GSVSCs are shared proportionally to their headrooms. On the other hand, it is observed from Fig. 8 (b) that the DC voltage profile decreases following the active power drop of the VSCs-3 and 5. Especially, DC voltage of the VSC-2 is near to the lower voltage limit. As shown in Fig 8 (c), the voltage profile decrease is mitigated after the autonomous control is activated to adjust the average voltage to the nominal value.

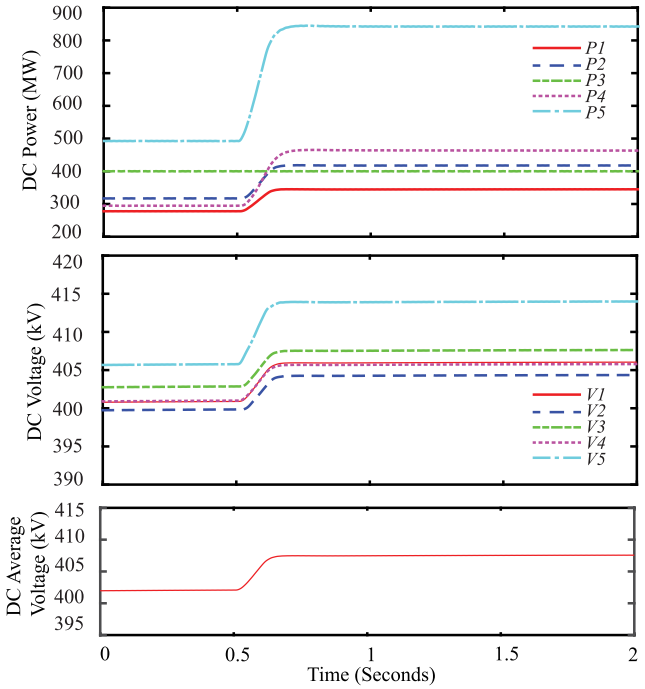

FIGURE 9. DC powers, voltages and average voltage of VSCs when VSC-5 power increases without automatic control. (a) VSC active powers; (b) VSC DC-side voltages; (c) VSC average voltage.

F. CASE E: THE DYNAMIC RESPONSE OF THE MTDC SYSTEM AFTER A DISTURBANCE WITH AND WITHOUT AUTOMATIC CONTROL

Similar with Case *A*, the active power of the VSC Station 5 increases from −500 MW to −850 MW when the time is 0.5 second. Due to space limitation, the autonomous control using the proposed Method II are shown in this case. The autonomous controls are enabled at the beginning. Figs. 9 and 10 show the behavior of the MTDC system without and with the autonomous controls respectively. It can be seen in Fig 10 that the voltage profile can mitigate the voltage increase and adjust the average voltage to the nominal value. In addition, the active powers of the GSVSCs in Fig. 10 are shared proportionally to their headrooms using

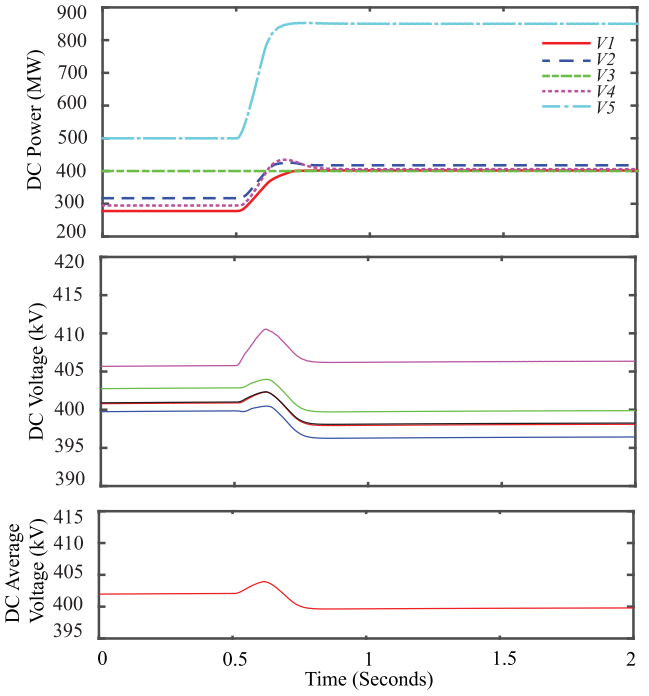

FIGURE 10. DC powers, voltages and average voltage of VSCs when VSC-5 power increases with automatic control. (a) VSC active powers; (b) VSC DC-side voltages; (c) VSC average voltage.

the proposed autonomous control. While the DC voltages and powers in Fig. 9 are not desirable without the proposed autonomous control.

V. CONCLUSION

In the presented paper, two adaptive voltage reference based droop control methods are proposed to regulate pilot (average) DC voltage and share converter power burden autonomously when integrating large-scale offshore wind. The presented Method I utilizes the DC grid lossy model with the local voltage droop control scheme, while the proposed Method II adopts an MPVDC strategy in the DC grid. The effectiveness of the presented autonomous control methods is verified using dynamic simulations under various disturbances, i.e., power variation, converter outage, and DC cable disconnection. Moreover, both $N-1$ and $N-2$ disturbances are included in the simulation studies. From the simulation results, it is shown that the proposed methods can realize converter power sharing and average DC voltage regulation simultaneously with very small errors. The proposed Method II is more accurate than the proposed Method I although it requires the communication of pilot voltage feedback signal among the VSC stations. Thus, the proposed Method I can also be regarded as a backup method during post-contingency primary communication loss. It is noted that both of the proposed control methods are autonomous as they do not need a centralized controller with global DC-grid power flow solution. Impact of adjusting DC voltage reference on the stability of the VSC-HVDC system will be the future work.

REFERENCES

[1] H. Dong, Z. Xu, P. Song, G. Tang, Q. Xu, and L. Sun, "Optimized power redistribution of offshore wind farms integrated VSC-MTDC transmissions after onshore converter outage," *IEEE Trans. Ind. Electron.*, vol. 64, no. 11, pp. 8948–8958, Nov. 2017.

[2] N. Fichaux, J. Wilkes, F. Van Hulle, and A. Cronin, "Oceans of opportunity: Harnessing Europe's largest domestic energy resource," Eur. Wind Energy Assoc., Brussels, Belgium, Tech. Rep. 41018647, Sep. 2009.

[3] G. Tang, Z. Xu, H. Dong, and Q. Xu, "Sliding mode robust control based active-power modulation of multi-terminal HVDC transmissions," *IEEE Trans. Power Syst.*, vol. 31, no. 2, pp. 1614–1623, Mar. 2016.

[4] WindEurope. (2019). *Offshore Wind in Europe, Key Trends and Statistics, 2018*. [Online]. Available: https://windeurope.org/wp-content/uploads/files/about-wind/statistics/WindEurope-Annual-Offshore-Statistics-2018.pdf

[5] N. Akbari, D. Jones, and R. Treloar, "A cross-European efficiency assessment of offshore wind farms: A DEA approach," *Renew. Energy*, vol. 151, pp. 1186–1195, May 2020.

[6] I. M. Sanz, B. Chaudhuri, and G. Strbac, "Inertial response from offshore wind farms connected through DC grids," *IEEE Trans. Power Syst.*, vol. 30, no. 3, pp. 1518–1527, May 2015.

[7] M. Guan, W. Pan, J. Zhang, Q. Hao, J. Cheng, and X. Zheng, "Synchronous generator emulation control strategy for voltage source converter (VSC) stations," *IEEE Trans. Power Syst.*, vol. 30, no. 6, pp. 3093–3101, Nov. 2015.

[8] P. Higgins and A. Foley, "The evolution of offshore wind power in the United Kingdom," *Renew. Sustain. Energy Rev.*, vol. 37, pp. 599–612, 2014.

[9] L. P. Kunjumuhammed, B. C. Pal, R. Gupta, and K. J. Dyke, "Stability analysis of a PMSG-based large offshore wind farm connected to a VSC-HVDC," *IEEE Trans. Energy Convers.*, vol. 32, no. 3, pp. 1166–1176, Sep. 2017.

[10] W. Du, Q. Fu, and H. Wang, "Comparing AC dynamic transients propagated through VSC HVDC connection with master–slave control versus DC voltage droop control," *IEEE Trans. Sustain. Energy*, vol. 9, no. 3, pp. 1285–1297, Jul. 2018.

[11] H. Li, C. Liu, G. Li, and R. Iravani, "An enhanced DC voltage droop-control for the VSC-HVDC grid," *IEEE Trans. Power Syst.*, vol. 32, no. 2, pp. 1520–1527, Mar. 2017.

[12] B. Li, Y. Liu, B. Li, and Y. Xue, "Research on the coordinated control of the true bipolar VSC-HVdc grid based on operating point optimization," *IEEE Trans. Ind. Electron.*, vol. 66, no. 9, pp. 6692–6702, Sep. 2019.

[13] H. Liu et al., "Small-signal analysis of DC microgrid and multi-objective optimization segmented droop control suitable for economic dispatch," *J. Mod. Power Syst. Clean Energy*, vol. 8, no. 3, pp. 564–572, May 2020.

[14] J. Beerten, D. Van Hertem, and R. Belmans, "VSC MTDC systems with a distributed DC voltage control—A power flow approach," in *Proc. IEEE Trondheim PowerTech*, Jun. 2011, pp. 1–6.

[15] W. Wang, Y. Li, Y. Cao, U. Häger, and C. Rehtanz, "Adaptive droop control of VSC-MTDC system for frequency support and power sharing," *IEEE Trans. Power Syst.*, vol. 33, no. 2, pp. 1264–1274, Mar. 2018.

[16] B. Li, Q. Li, Y. Wang, W. Wen, B. Li, and L. Xu, "A novel method to determine droop coefficients of DC voltage control for VSC-MTDC system," *IEEE Trans. Power Del.*, vol. 35, no. 5, pp. 2196–2211, Oct. 2020.

[17] S. G. Vennelaganti and N. R. Chaudhuri, "Stability criterion for inertial and primary frequency droop control in MTDC grids with implications on ratio-based frequency support," *IEEE Trans. Power Syst.*, vol. 35, no. 5, pp. 3541–3551, Sep. 2020, doi: 10.1109/TPWRS.2020.2976817.

[18] K. Rouzbehi, A. Miranian, J. I. Candela, A. Luna, and P. Rodriguez, "A generalized voltage droop strategy for control of multiterminal DC grids," *IEEE Trans. Ind. Appl.*, vol. 51, no. 1, pp. 607–618, Jan. 2015.

[19] W. Wang and M. Barnes, "Power flow algorithms for multi-terminal VSC-HVDC with droop control," *IEEE Trans. Power Syst.*, vol. 29, no. 4, pp. 1721–1730, Jul. 2014.

[20] B. Berggren, R. Majumder, C. Sao, and K. Linden, "Method and control device for controlling power flow within a DC power transmission network," WIPO Int. Publication Number WO 2012/000 549, Mar. 2012.

[21] N. R. Chaudhuri and B. Chaudhuri, "Adaptive droop control for effective power sharing in multi-terminal DC (MTDC) grids," *IEEE Trans. Power Syst.*, vol. 28, no. 1, pp. 21–29, Feb. 2013.

[22] A. Kirakosyan, E. F. El-Saadany, M. S. E. Moursi, and K. A. Hosani, "DC voltage regulation and frequency support in pilot voltage droop-controlled multiterminal HVdc systems," *IEEE Trans. Power Del.*, vol. 33, no. 3, pp. 1153–1164, Jun. 2018.

[23] J. Beerten and R. Belmans, "Analysis of power sharing and voltage deviations in droop-controlled DC grids," *IEEE Trans. Power Syst.*, vol. 28, no. 4, pp. 4588–4597, Nov. 2013.

[24] K. Rouzbehi, A. Miranian, A. Luna, and P. Rodriguez, "DC voltage control and power sharing in multiterminal DC grids based on optimal DC power flow and voltage-droop strategy," *IEEE J. Emerg. Sel. Topics Power Electron.*, vol. 2, no. 4, pp. 1171–1180, Dec. 2014.

[25] X. Li, L. Guo, C. Hong, Y. Zhang, Y. W. Li, and C. Wang, "Hierarchical control of multiterminal DC grids for large-scale renewable energy integration," *IEEE Trans. Sustain. Energy*, vol. 9, no. 3, pp. 1448–1457, Jul. 2018.

[26] M. A. Abdelwahed and E. F. El-Saadany, "Power sharing control strategy of multiterminal VSC-HVDC transmission systems utilizing adaptive voltage droop," *IEEE Trans. Sustain. Energy*, vol. 8, no. 2, pp. 605–615, Apr. 2017.

[27] A. Yogarathinam and N. R. Chaudhuri, "Stability-constrained adaptive droop for power sharing in AC-MTDC grids," *IEEE Trans. Power Syst.*, vol. 34, no. 3, pp. 1955–1965, May 2019.

[28] Y. Liu, T. C. Green, J. Wu, K. Rouzbehi, A. Raza, and D. Xu, "A new droop coefficient design method for accurate power-sharing in VSC-MTDC systems," *IEEE Access*, vol. 7, pp. 47605–47614, 2019.

[29] X. Ran, S. Miao, and Y. Wu, "Improved adaptive droop control design for optimal power sharing in VSC-MTDC integrating wind farms," *Energies*, vol. 8, no. 7, pp. 7100–7121, Jul. 2015.

[30] S. Song, R. A. McCann, and G. Jang, "Cost-based adaptive droop control strategy for VSC-MTDC system," *IEEE Trans. Power Syst.*, vol. 36, no. 1, pp. 659–669, Jan. 2021.

[31] Y. Zhang, A. M. Shotorbani, L. Wang, and W. Li, "Distributed voltage regulation and automatic power sharing in multi-terminal HVDC grids," *IEEE Trans. Power Syst.*, vol. 35, no. 5, pp. 3739–3752, Sep. 2020.

[32] S. Khan and S. Bhowmick, "A generalized power-flow model of VSC-based hybrid AC–DC systems integrated with offshore wind farms," *IEEE Trans. Sustain. Energy*, vol. 10, no. 4, pp. 1775–1783, Oct. 2019.

[33] Y. Wang, W. Wen, C. Wang, H. Liu, X. Zhan, and X. Xiao, "Adaptive voltage droop method of multiterminal VSC-HVDC systems for DC voltage deviation and power sharing," *IEEE Trans. Power Del.*, vol. 34, no. 1, pp. 169–176, Feb. 2019.

[34] Y. Wang et al., "DC voltage deviation-dependent voltage droop control method for VSC-MTDC systems under large disturbances," *IET Renew. Power Gener.*, vol. 14, no. 5, pp. 891–896, Apr. 2020.

[35] Y. Wang, F. Qiu, G. Liu, M. Lei, C. Yang, and C. Wang, "Adaptive reference power based voltage droop control for VSC-MTDC systems," *J. Mod. Power Syst. Clean Energy*, vol. 11, no. 1, pp. 381–388, Jan. 2023, doi: 10.35833/MPCE.2021.000307.

[36] A. Satish Kumar and B. Prasad Padhy, "Adaptive droop control strategy for autonomous power sharing and DC voltage control in wind farm-MTDC grids," *IET Renew. Power Gener.*, vol. 13, no. 16, pp. 3180–3190, Dec. 2019.

[37] Z. Wang, J. He, Y. Xu, and F. Zhang, "Distributed control of VSC-MTDC systems considering tradeoff between voltage regulation and power sharing," *IEEE Trans. Power Syst.*, vol. 35, no. 3, pp. 1812–1821, May 2020.

[38] S. Sahoo and S. Mishra, "A distributed finite-time secondary average voltage regulation and current sharing controller for DC microgrids," *IEEE Trans. Smart Grid*, vol. 10, no. 1, pp. 282–292, Jan. 2019.

[39] R. Han, L. Meng, J. M. Guerrero, and J. C. Vasquez, "Distributed nonlinear control with event-triggered communication to achieve current-sharing and voltage regulation in DC microgrids," *IEEE Trans. Power Electron.*, vol. 33, no. 7, pp. 6416–6433, Jul. 2018.

[40] Y. Dou, M. Chi, Z.-W. Liu, G. Wen, and Q. Sun, "Distributed secondary control for voltage regulation and optimal power sharing in DC microgrids," *IEEE Trans. Control Syst. Technol.*, vol. 30, no. 6, pp. 2561–2572, Nov. 2022.

[41] P. Rault et al., "Coordinated control for multi terminal DC grids connected to offshore wind farms," in *Proc. IEEE 17th Workshop Control Model. Power Electron. (COMPEL)*, Jun. 2016, pp. 1–8.

[42] O. Yadav, N. Kishor, and R. Negi, "Power imbalance sharing among the power converters in MTDC system," *Int. J. Electr. Power Energy Syst.*, vol. 109, pp. 584–596, Jul. 2019.

[43] J.-S. Kim, J.-Y. Park, Y.-J. Kim, and O. Gomis-Bellmunt, "Decentralized robust frequency regulation of multi-terminal HVDC-linked grids," *IEEE Trans. Power Syst.*, vol. 38, no. 4, pp. 3279–3292, Jul. 2023, doi: 10.1109/TPWRS.2022.3201316.
[44] Y. Zhang, X. Meng, A. M. Shotorbani, and L. Wang, "Minimization of AC–DC grid transmission loss and DC voltage deviation using adaptive droop control and improved AC–DC power flow algorithm," *IEEE Trans. Power Syst.*, vol. 36, no. 1, pp. 744–756, Jan. 2021, doi: 10.1109/TPWRS.2020.3020039.
[45] L. Xiao, Z. Xu, T. An, and Z. Bian, "Improved analytical model for the study of steady state performance of droop-controlled VSC-MTDC systems," *IEEE Trans. Power Syst.*, vol. 32, no. 3, pp. 2083–2093, May 2017.
[46] T. M. Haileselassie and K. Uhlen, "Impact of DC line voltage drops on power flow of MTDC using droop control," *IEEE Trans. Power Syst.*, vol. 27, no. 3, pp. 1441–1449, Aug. 2012.
[47] H. Saad, K. Jacobs, W. Lin, and D. Jovcic, "Modelling of MMC including half-bridge and full-bridge submodules for EMT study," in *Proc. Power Syst. Comput. Conf. (PSCC)*, Jun. 2016, pp. 1–7.
[48] C. Guo, P. Cui, and C. Zhao, "Optimization and configuration of control parameters to enhance small-signal stability of hybrid LCC-MMC HVDC system," *J. Mod. Power Syst. Clean Energy*, vol. 10, no. 1, pp. 213–221, Jan. 2022.
[49] X. Meng, J. Han, L. M. Bieber, L. Wang, W. Li, and J. Belanger, "A universal blocking-module-based average value model of modular multilevel converters with different types of submodules," *IEEE Trans. Energy Convers.*, vol. 35, no. 1, pp. 53–66, Mar. 2020.

YUANSHI ZHANG (Member, IEEE) received the B.Eng. and M.A.Sc. degrees from the Harbin Institute of Technology, China, in 2013 and 2015, respectively, and the Ph.D. degree from The University of British Columbia, Canada, in 2021. Since 2021, he has been an Assistant Professor with the School of Electrical Engineering, Southeast University, Nanjing, China. His current research interests include power system analysis, and modeling and control of modular-multilevel-converter-based high-voltage direct current transmission systems.

WENYAN QIAN received the B.Eng. degree in electrical engineering and automation from Nanjing Normal University, Nanjing, China, in 2021. She is currently pursuing the M.Eng. degree in electrical engineering with Southeast University, Nanjing. Her current research interests include optimal coordination control of ac/dc systems, power system analysis, and optimization and control of renewable energy power systems.

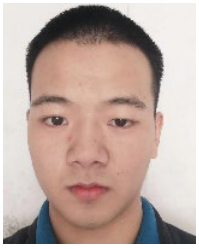

JUN SHAO received the bachelor's degree from the Wuhan University of Science and Technology, Wuhan, China, in 2023. He is currently pursuing the master's degree in electrical engineering from Nanjing Normal University. His research interests include HVdc converters and photovoltaic roof image recognition.

FEI ZHANG (Member, IEEE) received the B.S. and M.S. degrees in electrical engineering from Tsinghua University, Beijing, China, in 2009 and 2012, respectively, and the Ph.D. degree in electrical engineering from McGill University, Montreal, QC, Canada, in 2018. From 2018 to 2020, he was a specialist in modeling and electrical simulation with Opal-RT Technologies, Montreal, Canada. Since 2020, he has been an Assistant Professor with the School of Electrical Engineering, Southeast University, Nanjing, China. His research interests include HVdc converters, high-power electronics, and real-time simulation.

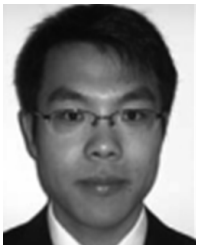

LIWEI WANG (Senior Member, IEEE) received the Ph.D. degree in electrical and computer engineering from The University of British Columbia, Vancouver, BC, Canada, in 2010. In August 2010, he joined the ABB Corporate Research Center, Västerås, Sweden, as a Scientist, and then as a Senior Scientist. In July 2014, he joined the School of Engineering, The University of British Columbia, Kelowna, BC, Canada, as an Assistant Professor. His research interests include power system modeling and simulation, electrical machines and drives, utility power electronics applications, and distributed generation.

QINRAN HU (Senior Member, IEEE) received the B.S. degree in electrical engineering from the Chien-Shiung Wu College, Southeast University, Nanjing, China, in 2010, and the M.S. and Ph.D. degrees in electrical engineering from the University of Tennessee, Knoxville, TN, USA, in 2013 and 2015, respectively. From 2015 to 2018, he was a Post-Doctoral Fellow with Harvard University, Cambridge, MA, USA. In October 2018, he joined the School of Electrical Engineering, Southeast University. He is also with the State Key Laboratory of Smart Grid Protection and Control, NARI Group Corporation. His research interests include power system optimization, demand aggregation, and virtual power plants.

WEI LI (Member, IEEE) received the B.Eng. degree from Zhejiang University, China, the M.Eng. degree from the National University of Singapore, Singapore, and the Ph.D. degree from McGill University, Canada. He is currently a Senior Power System Simulation Specialist with OPAL-RT Technologies, Montreal. His fields of interest are power electronics, renewable energy, and distributed generation. His current research interests include real-time simulation and controls of modular multilevel converter HVdc systems and FACTS devices.